IUST
Iran University of Science and Technology

Iranian Journal of Electrical and Electronic Engineering

Journal Homepage: ijeee.iust.ac.ir

Research Paper

A Laplacian Approach to Locate Source of Forced Oscillations Under Resonance Conditions Based on Energy-Driven Multilateral Interactive Pattern

A. Hesami Naghshbandy*(C.A.), K. Naderi*, and U. D. Annakkage**

Abstract: The most challenging circumstance of forced oscillations (FOs) is when the power system is forced to oscillate at its natural frequencies. This paper uses a novel PMU data-driven mechanism to pinpoint the source of such phenomena under resonance. Following the detection of FOs, the instantaneous changes in the output power and angular velocity of the rotors are calculated. Accordingly, an energy-driven multilateral interaction pattern is obtained for all synchronous generators. Next, an appropriate positive weighted undirected graph is constructed through these functional patterns based on the spectral graph theory. These quantitative indicators are then analyzed through the eigenvalue spectrum of the normalized Laplacian matrix of the system graph reduced to the internal generator buses. Finally, the smallest value in eigenvectors corresponding to the two largest eigenvalues reveals the location of the source. The proposed methodology's validation and verification studies have been performed on the WECC 3-machine 9-bus and New England 10-machine 39-bus benchmark power systems modeled in the Real-Time Digital Simulator (RTDS) and then analyzed in the MATLAB environment. The proposed methodology revealed to be fast and accurate in locating the source of FOs under challenging resonance situations with promising results while addressing the generator side origins.

Keywords: Forced Oscillation, Laplacian Matrix, Multilateral Interactive Pattern, Resonance, Source Locating, Spectral Graph Theory.

Nomenclature

ω_i	Angular velocity of the *i*-th rotor relative to synchronous frame of reference.
$\hat{\omega}_i$	Angular velocity of the *i*-th rotor with respect to COI-reference frame.
δ_{COI}	COI angle.
ω_{COI}	COI speed.
θ_{I_i}	Current angle of the corresponding PMU bus *i* with respect to synchronous frame of reference.
$\hat{\theta}_{I_i}$	Current angle of the corresponding PMU bus *i* with respect to COI-reference frame.
I_i	Current magnitude of the corresponding PMU bus *i*.
D_i	Damping coefficient of the *i*-th generator in PU.
P_{e_i}	Electrical power output of the *i*-th generator.
H_i	Inertia constant of the *i*-th generator in seconds or MW.s/MVA.
P_i	Injected power into bus *i*.
$\bar{E}_i$	Internal voltage of the *i*-th generator.
$V_{KE_i}(\tilde{\omega})$	Kinetic energy function of the *i*-th generator.
P_{m_i}	Mechanical power input to the *i*-th generator.

Iranian Journal of Electrical and Electronic Engineering, 2022.
Paper first received 13 March 2022, revised 04 June 2022, and accepted 06 June 2022.
* The authors are with the Department of Electrical Engineering, University of Kurdistan, Sanandaj, Iran.
E-mails: hesami@uok.ac.ir and ka.naderi@uok.ac.ir.
** The author is with the Department of Electrical and Computer Engineering, University of Manitoba, Winnipeg, Manitoba, Canada.
E-mail: udaya.annakkage@umanitoba.ca.
Corresponding Author: A. Hesami Naghshbandy.
https://doi.org/10.22068/IJEEE.18.3.2455

M_i	Moment of inertia (angular momentum) of the *i*-th generator in kg.m^2.
m	Number of generators.
n	Number of system buses.
$V_{PE_i}\left(\hat{\delta}\right)$	Potential energy function of the *i*-th generator.
δ_{ij}	Relative *i*-th and *j*-th rotors angle.
ω_{ij}	Relative *i*-th and *j*-th rotors speed.
$\hat{\delta}_i$	Relative rotor angle of the *i*-th generator with respect to COI-reference frame.
δ_i	Rotor angle of the *i*-th generator relative to synchronous frame of reference.
R_{s_i}	Stator resistance of the *i*-th generator.
X_{q_i}	Steady-state quadrature axis synchronous reactance of the *i*-th generator.
ω_s	Synchronous frame of reference angular velocity ($2pf_s$) in (elec.rad/s).
f_s	The power system nominal frequency equal to 50 Hz.
T	Time in seconds.
$V_{KE_T}\left(\tilde{\omega}\right)$	Total kinetic energy function.
$V_{PE_T}\left(\hat{\delta}\right)$	Total potential energy function.
$V_T\left(\tilde{\omega},\hat{\delta}\right)$	Total transient energy function.
G_{ij}	Transfer conductance between *i*-th and *j*-th generators.
B_{ij}	Transfer susceptance between *i*-th and *j*-th generators.
$V_i\left(\tilde{\omega},\hat{\delta}\right)$	Transient energy function of the *i*-th generator.
θ_{V_i}	Voltage angle of the corresponding PMU bus *i* with respect to synchronous frame of reference.
$\hat{\theta}_{V_i}$	Voltage angle of the corresponding PMU bus *i* with respect to COI-reference frame.
V_i	Voltage magnitude of the corresponding PMU bus *i*.

1 Introduction

PHASOR measurement units (PMUs) use state-of-the-art digital signal processors. They can provide an invaluable wide-area snapshot of synchronized measurements of the phasors, frequency, and the rate of change of frequency (ROCOF) of the voltage and current signals across the power system. The typical sampling rate of PMUs is 30–60 frames per second. PMUs are widely deployed on strategic spots over power systems [1]. They cause full observability of system states and dynamic behaviors in real-time, including forced oscillations (FOs), referring to the power system's response to a periodic external perturbation which is a significant threat to the system security [2]. The power system is inevitably forced into a pervasive oscillating behavior in response to the unsatisfactory nonlinear performance of an apparatus such as synchronous generator AVR [3], over-excitation limiters (OEL) [4], modulated steam turbine extraction-control valve reference [5], and power system stabilizer (PSS) [6]. An external or non-modeled time-dependent force can appear in infinitely different forms, including sinusoids and stable limit cycles (periodic motions) induced by supercritical Poincare-Andropov-Hopf bifurcation [7], and pulse waveform.

FOs swiftly pervade the whole power system and cast a shadow over its components and variables. They will continue to exist as long as appropriate action is not taken. Source frequency is one of the critical factors affecting the magnitude of FOs. Due to the resonance phenomenon, FOs can be amplified to manifest their negative effects in places far away from the actual source [8]. Therefore, a power system immersed in FOs is potentially in danger of blackouts and eventually partial or complete collapse. The most effective countermeasure to deal with such a situation is to locate the source of the periodic disturbance and further implement an appropriate remedial strategy as immediately as possible, including overhauling or detaching the damaged apparatus.

Energy is a fundamentally important framework in our perception of all physical phenomena. Lyapunov functions or synonymously Transient Energy Function (TEF) have been used in various contexts of power systems as the sum of kinetic and potential energies of the post-disturbance status [9]. Over the last few years, some research has been developed on the issue of locating the sources of FOs based on the concept of energy. To the best of our knowledge, the first study on FOs source location problem based on energy approach is proposed in [10] assuming lossless network and constant power static load model. According to [11], the variation of energy flow across network cut-sets can be used to identify the location of the source. However, the transmission losses are neglected. A derivation of the energy method entitled dissipating energy flow (DEF) has been used in [12-14] to locate poorly damped natural and FOs sources by using PMU measurements. This approach is merely applicable in the case of radial power systems. Besides, network losses and load characteristics severely affect its performance.

In this paper, a well-established function is proposed to extract the multilateral interactive patterns based on the difference in instantaneous changes in the electrical power provided by the synchronous generators and the angular velocities of the rotors. Subsequently, a complete positive undirected graph weighted on this basis is introduced. In the meantime, any dependence on the transmission network is removed. Relying on the spectral graph theory, the source location problem is formulated as a normalized Laplacian matrix that carries the power system's incredibly momentous properties through Eigen analysis of the assigned graph. Ultimately the source location is revealed through the smallest value in eigenvectors corresponding to the two

largest eigenvalues of the Laplacian matrix.

The remainder of the paper proceeds as follows. Section 2 provides a detailed insight into the proposed multilateral interactive pattern approach derivative from the multi-generator power system's transient energy function (TEF) results. The spectral graph theory studies on the constructed positive weighted undirected graph concerning the eigenvalue spectrum of the normalized Laplacian matrix are discussed in Section 3 to locate the source of FOs under problematic resonance circumstances in a reliable manner. The fourth section concerns the performance and effectiveness of the methodology used for this study on the WECC 3-machine 9-bus and New England 10-machine 39-bus benchmark power systems. Finally, conclusions are drawn in Section 5.

2 The Energy-Driven Multilateral Interactive Pattern

2.1 Energy Function Analysis for A Multi-Machine Power System

In this section, we rebuilt the rotor potential energy changes through transient energy function (TEF), which is reported in [15] for a multi-machine individual power system that is reduced to the internal nodes of the generators.

According to the following state equations, the *i*-th Individual synchronous generator operates under Newton's second law of angular motion in a multi-machine power system.

$$\dot{\delta}_i = \omega_i \tag{1}$$

$$\frac{2H_i}{\omega_s}\frac{d^2\delta_i}{dt^2} + D_i\frac{d\delta_i}{dt} = P_{m_i} - P_{e_i}, \quad i = 1,\ldots,m \tag{2}$$

where,

$$M_i \triangleq \frac{2H_i}{\omega_s} \tag{3}$$

The angle and angular velocity of the rotor in (1) and (2) are considered relative to the synchronous frame of reference. It is convenient to redefine all variables relative to a center of inertia (COI)-reference frame as follows.

$$\delta_{COI} \triangleq \frac{1}{M_T}\sum_{i=1}^{m} M_i\delta_i \Rightarrow \dot{\delta}_{COI} = \frac{1}{M_T}\sum_{i=1}^{m} M_i\dot{\delta}_i \tag{4}$$

$$\omega_{COI} \triangleq \frac{1}{M_T}\sum_{i=1}^{m} M_i\omega_i \Rightarrow \dot{\omega}_{COI} \triangleq \frac{1}{M_T}\sum_{i=1}^{m} M_i\dot{\omega}_i \tag{5}$$

$$f_{COI} \triangleq \frac{1}{M_T}\sum_{i=1}^{m} M_i f_i \Rightarrow \dot{f}_{COI} \triangleq \frac{1}{M_T}\sum_{i=1}^{m} M_i \dot{f}_i \tag{6}$$

where,

$$M_T \triangleq \sum_{i=1}^{m} M_i \tag{7}$$

New angles and angular velocities with respect to the COI-reference frame are defined as follows

$$\hat{\delta}_i \triangleq \delta_i - \delta_{COI} \tag{8}$$

$$\tilde{\omega}_i \triangleq \omega_i - \omega_{COI} \tag{9}$$

$$\tilde{f}_i \triangleq f_i - f_{COI} \tag{10}$$

An individual generator G_i is connected to its terminal bus via an impedance and then interacts with other generators through transmission networks and loads. A schematic of such a description, aiming to focus on the rotor behavior of the generators, summarizes the entire network in the internal buses of the generators, as shown in Fig. 1.

The electrical output active power P_{e_i} of the outgoing generator line G_i can be described as a function of its internal voltage and output current values as

$$P_{e_i} = \mathrm{Re}\left(\bar{E}_i\bar{I}_i^*\right) \tag{11}$$

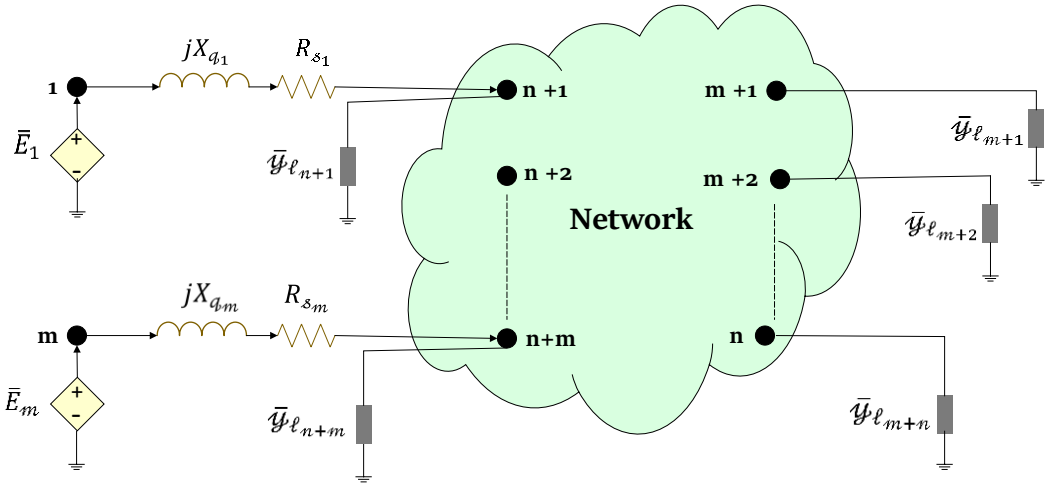

Fig. 1 Schematic diagram of a multi-machine power system.

where,

$$\bar{E}_i = E_i e^{j\hat{\delta}_i} \tag{12}$$

$$\bar{I}_i = \sum_{j=1}^{m} \bar{Y}_{aug_{ij}} \bar{E}_j \tag{13}$$

Also $\bar{Y}_{aug_{ij}} = \left(G_{aug_{ij}} + B_{aug_{ij}}\right)$ is related to *i*-th row and *j*-th column of the augmented network admittance matrix to the generators' internal nodes, equal to the Thevenin-equivalent admittance between *i*-th and *j*-th internal buses. By substituting (12) and (13) into (11) and then expanding and applying further simplifications, we get

$$\begin{aligned} P_{e_i} &= \mathrm{Re}\left(E_i e^{j\hat{\delta}_i} \sum_{j=1}^{m} \bar{Y}^*_{aug_{ij}} \bar{E}^*_j \right) \\ &= \mathrm{Re}\left(E_i e^{j\hat{\delta}_i} \sum_{j=1}^{m} \left(G_{aug_{ij}} - jB_{aug_{ij}}\right) E_j e^{-j\hat{\delta}_j} \right) \\ &= \mathrm{Re}\left(\sum_{j=1}^{m} \left(G_{aug_{ij}} - jB_{aug_{ij}}\right) E_i E_j \left(\cos\left(\hat{\delta}_i - \hat{\delta}_j\right) + j\sin\left(\hat{\delta}_i - \hat{\delta}_j\right)\right) \right) \\ &= \sum_{j=1}^{m} E_i E_j \left(G_{aug_{ij}} \cos\left(\delta_{ij}\right) + B_{aug_{ij}} \sin\left(\delta_{ij}\right)\right) \\ &= E_i^2 G_{aug_{ij}} + \sum_{\substack{j=1 \\ j\neq i}}^{m} \left(C_{aug_{ij}} \sin\left(\delta_{ij}\right) + D_{aug_{ij}} \cos\left(\delta_{ij}\right)\right) \end{aligned} \tag{14}$$

where $C_{aug_{ij}} = E_i E_j B_{aug_{ij}}$ and $D_{aug_{ij}} = E_i E_j G_{aug_{ij}}$ and δ_{ij} is the relative angle of the considered generator rotor with other existing generators and is defined as follows

$$\delta_i - \delta_j = \hat{\delta}_i - \hat{\delta}_j \triangleq \delta_{ij}, \qquad j = (1,...,m) \neq i \tag{15}$$

By defining $P_i \triangleq P_{m_i} - E_i^2 G_{aug_{ij}}$, and ignoring the impact of damping windings, we get

$$\begin{aligned} M_i \frac{d^2\hat{\delta}_i}{dt^2} &= P_i - \sum_{\substack{j=1 \\ j\neq i}}^{m} \left(C_{aug_{ij}} \sin\left(\delta_{ij}\right) + D_{aug_{ij}} \cos\left(\delta_{ij}\right)\right) - \frac{M_i}{M_T} P_{COI} \\ &\triangleq f_i\left(\hat{\delta}_i\right) \end{aligned} \tag{16}$$

where

$$P_{COI} = \sum_{i=1}^{m} P_i - 2\sum_{i=1}^{m-1} \sum_{j=i+1}^{m} D_{aug_{ij}} \cos\left(\delta_{ij}\right) \tag{17}$$

$$M_i \frac{d\tilde{\omega}_i}{dt} = f_i\left(\hat{\delta}_i\right) \Rightarrow dt = \frac{M_i d\tilde{\omega}_1}{f_i\left(\hat{\delta}_i\right)} = \frac{d\hat{\delta}_i}{\tilde{\omega}_i} \tag{18}$$

$$\begin{aligned} V_T\left(\tilde{\omega}, \hat{\delta}\right) &= \frac{1}{2}\sum_{i=1}^{m} M_i \tilde{\omega}_i^{\,2} - \sum_{i=1}^{m} \int_{\hat{\delta}_i^o}^{\hat{\delta}_i} f_i\left(\hat{\delta}_i\right) d\hat{\delta}_i \\ &= \frac{1}{2}\sum_{i=1}^{m} M_i \tilde{\omega}_i^{\,2} - \sum_{i=1}^{m} \int_{\hat{\delta}_i^o}^{\hat{\delta}_i} P_i\left(\hat{\delta}_i\right) d\hat{\delta}_i \\ &\quad - \sum_{i=1}^{m-1} \sum_{j=i+1}^{m} \left(C_{aug_{ij}} \left(\cos\left(\delta_{ij}\right) - \cos\left(\delta_{ij}^o\right)\right) \right. \\ &\qquad \left. + \int_{\hat{\delta}_i^o + \hat{\delta}_j^o}^{\hat{\delta}_i + \hat{\delta}_j} D_{aug_{ij}} \cos\left(\delta_{ij}\right) d\left(\hat{\delta}_i + \hat{\delta}_j\right) \right) \end{aligned} \tag{19}$$

where

$$V_{KE_i}\left(\tilde{\omega}\right) = \frac{1}{2} M_i \tilde{\omega}_i^{\,2} \tag{20}$$

where $V_{KE_i}\left(\tilde{\omega}\right)$ demonstrates the kinetic energy change of the *i*-th generator rotor relative to the COI-reference frame, which is a function of only the generator angular velocity and is not the subject of this paper.

$$\begin{aligned} V_{PE}\left(\hat{\delta}\right) &= -\sum_{i=1}^{m} \int_{\hat{\delta}_i^o}^{\hat{\delta}_i} P_i\left(\hat{\delta}_i\right) d\hat{\delta}_i \\ &\quad - \sum_{i=1}^{m-1} \sum_{j=i+1}^{m} \left(C_{aug_{ij}} \left(\cos\left(\delta_{ij}\right) - \cos\left(\delta_{ij}^o\right)\right) \right. \\ &\qquad \left. + \int_{\hat{\delta}_i^o + \hat{\delta}_j^o}^{\hat{\delta}_i + \hat{\delta}_j} D_{aug_{ij}} \cos\left(\delta_{ij}\right) d\left(\hat{\delta}_i + \hat{\delta}_j\right) \right) \end{aligned} \tag{21}$$

It is worth mentioning that $V_{PE_i}\left(\hat{\delta}\right)$ is a function of only the generator angles and consists of the following terms

1- $\sum_{i=1}^{m} \int_{\hat{\delta}_i^o}^{\hat{\delta}_i} P_i\left(\hat{\delta}_i\right) d\hat{\delta}_i$ demonstrates the change in the total potential energy of the rotors relative to the COI-reference frame.

2- $\sum_{i=1}^{m-1} \sum_{j=i+1}^{m} \left(C_{aug_{ij}} \left(\cos\left(\delta_{ij}\right) - \cos\left(\delta_{ij}^o\right)\right)\right)$ demonstrates the magnetic energy stored in the Thevenin-equivalent branches.

3- $\sum_{i=1}^{m-1} \sum_{j=i+1}^{m} \left(\int_{\hat{\delta}_i^o + \hat{\delta}_j^o}^{\hat{\delta}_i + \hat{\delta}_j} D_{aug_{ij}} \cos\left(\delta_{ij}\right) d\left(\hat{\delta}_i + \hat{\delta}_j\right) \right)$ demonstrates the dissipation energy changes of the Thevenin-equivalent branches.

2.2 Real-Time Estimation of Internal Voltage and Power Angle of Generators

In this methodology, the PMU measurements of all generator's terminals are used to estimate the internal voltages of the generators and the angles of the rotors. We use the classic generator model as shown in Fig. 2.

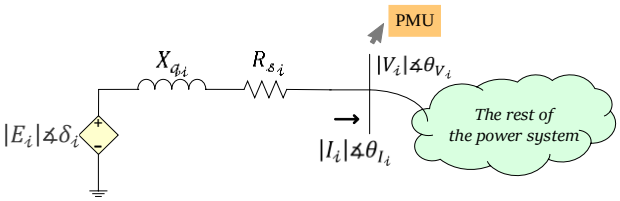

Fig. 2 Synchronous generator equivalent circuit.

We apply Kirchhoff's Voltage Law from the bus containing the PMU to the internal voltage of the generator as follows.

$$\delta_i - \delta_j = \hat{\delta}_i - \hat{\delta}_j \triangleq \delta_{ij}, \quad j = (1,...,m) \neq i \tag{22}$$

$$\delta_i = arg\left(\left(\bar{V}_i + \left(R_{s_i} + jX_{s_i}\right) \times \bar{I}_i\right)\right) \tag{23}$$

It is necessary to mention that the synchronous generator's apparent power rating is considered the apparent base power of the subsystem. All angles, including PMUs, are measured relative to the COI reference.

2.3 The Proposed Methodology

The main idea of the work is introduced in this subsection. Assuming the interconnectedness and stability of the power system, synchronous generators are operated under a multilateral interactive behavior. In fact, changing the point of operation or the occurrence of defects and anomalies in any of them affects all the other generators. The ultimate goal of this multilateral cooperation is to maintain the security and stability of the whole power system so that the required energy of the network is always provided. Therefore, following the emergence of a forced oscillation in one of the synchronous generators, other generators in the network are affected by this condition.

During the presence of a forced oscillation in the system, the total potential energy changes of the rotors of all synchronous generators can be expressed as follows.

$$V_{PE_T}\left(\hat{\delta}\right) = \sum_{i=1}^{m} \int_{\hat{\delta}_i^o}^{\hat{\delta}_i} \Delta P_i\left(\hat{\delta}_i\right) d\hat{\delta}_i \tag{24}$$

Assuming a mathematical function $u = \varphi(t)$, according to integration by Reverse Chain rule as follows.

$$du = \varphi'(t)\,dt \tag{25}$$

$$\int_a^b f\left(\varphi(t)\right)\varphi'(t)\,dt = \int_a^b (fo\varphi)'(t)\,dt = fo\varphi(b) - fo\varphi(a)$$

$$= f\left(\varphi(b)\right) - f\left(\varphi(a)\right) = \int_{\varphi(a)}^{\varphi(b)} f(u)\,du \tag{26}$$

We get

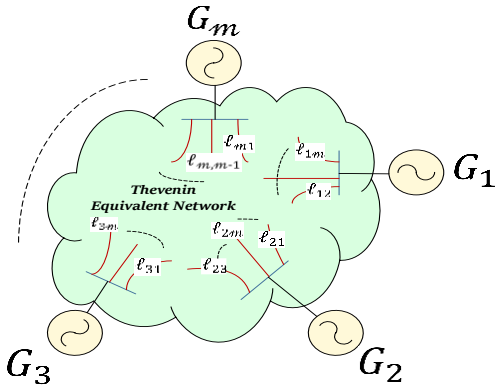

Fig. 3 Schematic diagram of a reduced power system.

$$\sum_{i=1}^{m} \int_{\hat{\delta}_i^o}^{\hat{\delta}_i} \Delta P_i\left(\hat{\delta}_i\right) d\hat{\delta}_i = \sum_{i=1}^{m} \int_{t^o}^{t} \Delta P_i(t)\,\tilde{\omega}_i(t)\,dt \tag{27}$$

The difference in changes in output electrical powers and angular velocities difference between any two generators at any point in time relative to the previous moment is defined as follows.

$$\omega_{ij}(t) = \tilde{\omega}_i(t) - \tilde{\omega}_j(t) \tag{28}$$

$$\Delta P_{ij}(t) = \Delta P_i(t) - \Delta P_j(t) \tag{29}$$

Relying on the fact that the sum of the changes in the output power flow of the generators is zero, as follows

$$\Delta P_i(t) = -\sum_{\substack{j=1 \\ j\neq i}}^{m} \left(\Delta P_j(t)\right) \tag{30}$$

Fig. 3 shows the system reduced graph to the generators' internal buses that seem to be connected by a special equivalent Thevenin circuits.

In the following, the Multilateral Interactive pattern of generators is formulated as follows:

$$\sum_{i=1}^{m}\left(\int_{t^o}^{t} \Delta P_i(t)\,\tilde{\omega}_i(t)\,dt\right) = \int_{t^o}^{t} \sum_{i=1}^{m}\left(\Delta P_i(t)\,\tilde{\omega}_i(t)\right)dt$$

$$= \frac{1}{2m}\left(\int_{t^o}^{t} 2m \sum_{i=1}^{m}\left(\Delta P_i(t)\,\tilde{\omega}_i(t)\right)dt\right)$$

$$= \frac{1}{2m}\left[\int_{t^o}^{t}\left((m-1)\sum_{i=1}^{m}\left(\Delta P_i(t)\,\tilde{\omega}_i(t)\right) + \sum_{i=1}^{m}\left(\Delta P_i(t)\,\tilde{\omega}_i(t)\right)\right.\right.$$

$$\left.\left. + (m-1)\sum_{i=1}^{m}\left(\Delta P_i(t)\,\tilde{\omega}_i(t)\right) + \sum_{i=1}^{m}\left(\Delta P_i(t)\,\tilde{\omega}_i(t)\right)\right)dt\right]$$

$$= \frac{1}{2m}\left[\int_{t^o}^{t}\left(\sum_{\substack{i=1 \\ j\neq i}}^{m}\sum_{j=1}^{m}\left(\Delta P_i(t)\,\tilde{\omega}_i(t)\right) - \sum_{\substack{i=1 \\ j\neq i}}^{m}\sum_{j=1}^{m}\left(\Delta P_i(t)\,\tilde{\omega}_i(t)\right)\right.\right.$$

$$\left.\left. - \sum_{\substack{i=1 \\ j\neq i}}^{m}\sum_{j=1}^{m}\left(\Delta P_i(t)\,\tilde{\omega}_i(t)\right) + \sum_{\substack{i=1 \\ j\neq i}}^{m}\sum_{j=1}^{m}\left(\Delta P_i(t)\,\tilde{\omega}_i(t)\right)\right)dt\right]$$

$$
\begin{aligned}
&= \frac{1}{2m}[\int_{t^o}^{t}\sum_{i=1}^{m}\sum_{\substack{j=1\\ j\neq i}}^{m}\big(\Delta P_i(t)\tilde{\omega}_i(t)-\Delta P_i(t)\tilde{\omega}_i(t) \\
&\qquad -\Delta P_i(t)\tilde{\omega}_i(t)+\Delta P_i(t)\tilde{\omega}_i(t)\big)dt] \\
&= \frac{1}{2m}[\int_{t^o}^{t}\sum_{i=1}^{m}\sum_{\substack{j=1\\ j\neq i}}^{m}\big(\big(\Delta P_i(t)-\Delta P_i(t)\big)\tilde{\omega}_i(t) \\
&\qquad -\big(\Delta P_i(t)-\Delta P_i(t)\big)\tilde{\omega}_i(t)\big)dt] \\
&= \frac{1}{2m}\left(\int_{t^o}^{t}\sum_{i=1}^{m}\sum_{\substack{j=1\\ j\neq i}}^{m}\big(\big(\Delta P_i(t)-\Delta P_i(t)\big)\big(\tilde{\omega}_i(t)-\tilde{\omega}_i(t)\big)\big)dt\right) \\
&= \frac{1}{2m}\left(\int_{t^o}^{t}\sum_{i=1}^{m}\sum_{\substack{j=1\\ j\neq i}}^{m}\big(\Delta P_{ij}(t)\omega_{ij}(t)\big)dt\right) \\
&= \frac{1}{m}\left(\sum_{i=1}^{m-1}\sum_{j=i+1}^{m}\left(\int_{t^o}^{t}\big(\Delta P_{ij}(t)\omega_{ij}(t)\big)dt\right)\right) \\
&= \sum_{i=1}^{m-1}\sum_{j=i+1}^{m}\left(\frac{1}{m}\int_{t^o}^{t}\big(\Delta P_{ij}(t)\omega_{ij}(t)\big)dt\right) \\
&= \sum_{i=1}^{m-1}\sum_{j=i+1}^{m}\left(\frac{2\pi}{m}\int_{t^o}^{t}\big(\Delta P_{ij}(t)\,f_{ij}(t)\big)dt\right) \qquad (31)
\end{aligned}
$$

In the following, the obtained result is used as the weighting coefficients of a graph.

3 Spectral Graph Theory Analysis

Spectral graph theory starts by defining matrices associated with the reduced power system graphs, namely, the adjacency matrix and the Laplacian matrix. After obtaining the eigenvalues and eigenvectors of such matrices, the general theme is that we are looking to discover the hidden structural properties (spectra) in the graph [16]. The power system is modelled as a positive weighted undirected graph $G = (V, E)$ with vertex set $v = \{v_1, v_2, \ldots, v_m\}$ for all internal generator buses. Each edge between two vertices v_i and v_j carries a non-negative weight w_{ij}. Using the bilateral interactive energy measure $BIE(v_i, v_j)$ for each pair of vertices $(1 \le i, j \le m)$, a weighted adjacency matrix W can be constructed as

$$
W(G) = \begin{bmatrix} 0 & w_{12} & \cdots & w_{1m} \\ w_{21} & 0 & \cdots & w_{2m} \\ \vdots & \vdots & \ddots & \vdots \\ w_{m1} & w_{m2} & \cdots & 0 \end{bmatrix} \qquad (32)
$$

where entries are defined as follows

$$
w_{ij} = \begin{cases} e^{-BIE(v_i,v_j)^2}, & \text{if } i \neq j \\ 0, & \text{otherwise} \end{cases} \qquad (33)
$$

where

$$
BIE(v_i, v_j) = \frac{2\pi}{m}\int_{t^o}^{t}\Big(\big|\Delta P_{ij}(t)\, f_{ij}(t)\big|\Big)dt \qquad (34)
$$

The main diagonal comprises purely zero arrays. Since the graph G is undirected (i.e., all of its branches are bidirectional) then $w_{ij} = w_{ji}$, which implies that the weighted adjacency matrix is symmetric. The degree matrix $\mathcal{D}$ is defined as

$$
\mathcal{D}(G) = \mathrm{diag}\big(d(v_1), d(v_2), \ldots, d(v_m)\big) \qquad (35)
$$

where $d(v_i)$ is the sum of the weights of the branches adjacent to v_i and can be defined as follows:

$$
d(v_i) = \sum_{i=1}^{m} w_{ij} \qquad (36)
$$

The normalized adjacency matrix is defined as

$$
\tilde{W} = \mathcal{D}^{-\frac{1}{2}} W \mathcal{D}^{-\frac{1}{2}} \qquad (37)
$$

where

$$
\mathcal{D}^{-\frac{1}{2}} = \begin{bmatrix} \frac{1}{\sqrt{d(v_1)}} & 0 & \cdots & 0 \\ 0 & \frac{1}{\sqrt{d(v_2)}} & \cdots & 0 \\ \vdots & \vdots & \ddots & \vdots \\ 0 & 0 & \cdots & \frac{1}{\sqrt{d(v_m)}} \end{bmatrix} \qquad (38)
$$

The Normalized Laplacian matrix, which carries the spectral information of the graph, is obtained as follows.

$$
\tilde{L} = I - \tilde{W} = \mathcal{D}^{-\frac{1}{2}}(\mathcal{D} - W)\mathcal{D}^{-\frac{1}{2}} = \mathcal{D}^{-\frac{1}{2}} L \mathcal{D}^{-\frac{1}{2}} \qquad (39)
$$

where $L = \mathcal{D} - W$ is the unnormalized Laplacian matrix. The normalized Laplacian matrix is positive and semi-definite and has m non-negative real-valued eigenvalues in the following order.

$$
0 = \lambda_1 \le \ldots \le \lambda_m \le 2 \qquad (40)
$$

It is worth mentioning that

$$
d(v_i)_{avg} \le \lambda_{max} \le d(v_i)_{max} \qquad (41)
$$

Finally, the smallest value of eigenvectors corresponding to the largest and second-largest eigenvalues reveals the location of the FOs source.

4 Numerical Test Results

This section implements the proposed methodology

on the WECC 3-machine 9-bus and New England 10-machine 39-bus benchmark power systems modeled in the RTDS simulator to generate the required simulation data. The PMUs monitor the system simultaneously at a sampling rate of 60 samples per second. All the PMUs contain Gaussian noises (SNR = 40 dB) to comply with real-world applications. Different scenarios of forced oscillation occurrence, including limit cycle and sinusoidal, have been investigated, during each of which a specific generator is considered as the source of FOs with a specified amount of frequency. The generators' damper winding has been neglected to achieve the most severe oscillating events. In this study, the generators are not equipped with any power system stabilizers (PSS) to obtain the intended poorly-damped oscillatory behaviors. The preceding data-processing procedures are implemented using MATLAB R2019b on a computer with a 3.4 GHz processor and 8 GB of memory.

4.1 Case Study 1: WECC 3-Machine 9-Bus Benchmark Power System

In order to have a better visual perception of the simulation results, we have chosen this small system. Network details, including a single-line diagram, are available in reference [17]. Following a small signal disturbance in the network, PMU datasets have been used to estimate critical dominant oscillation information. An instantaneous pulse with an amplitude of 0.1 per unit has been injected into the input mechanical torque of Generator 1. Fig. 4 shows the output powers of the generators following this situation.

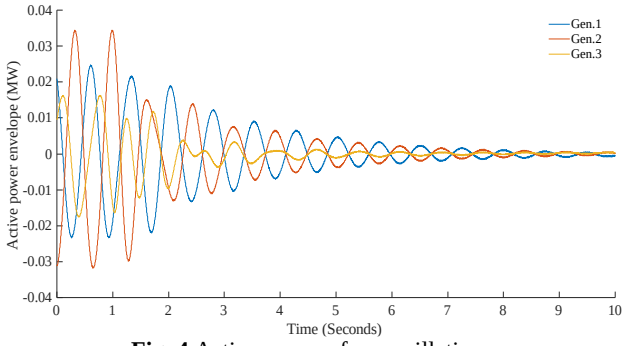

Fig. 4 Active powers free oscillation.

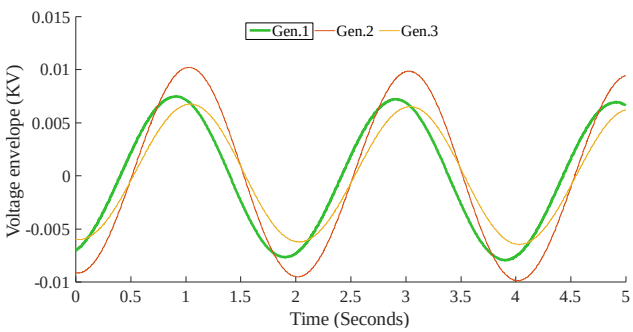

Fig. 6 Generator terminal buses voltage envelopes: Scenario 1.

Spectrum analysis results on the active power signals reveal that the system is dominated by two electromechanical modes, including a local mode with a frequency of 2.133 Hz related to generators 2 and 3 and a local mode with a frequency of 1.39 Hz related to generator one against the other two generators as can be seen in Fig. 5.

In order to study the forced oscillations under the harsh resonance conditions, a persistent periodic disturbance with the system resonant frequency has been injected into the input mechanical torque of one of the synchronous generators as $\tau_m = \tau_m{}^o + \alpha \sin(2\pi f_d t)$ each in a particular scenario, in which α and f_d are the magnitude and frequency of the driven source, respectively. Four scenarios, including one non-resonance and three resonance cases on this system, have been investigated.

4.1.1 Scenario 1: Non-Resonance

To evaluate the capability of the proposed method in non-resonant conditions for a small system, an arbitrary disturbance with a frequency of 0.5 Hz has been injected into the mechanical torque of generator one as $\tau_{m_1} = \tau_{m_1}^o + 0.1\sin(3.141\times t)$. The voltage and frequency envelopes of all generator terminal buses measured by PMUs for this disturbance are shown in Figs. 6 and 7.

As can be seen, none of the amplitudes of frequency and voltage magnitude oscillations related to the source generator is maximum. Generator 2 has experienced the most amplitudes of both frequency and voltage oscillations. Fig. 8 shows Welch's result with a 95%

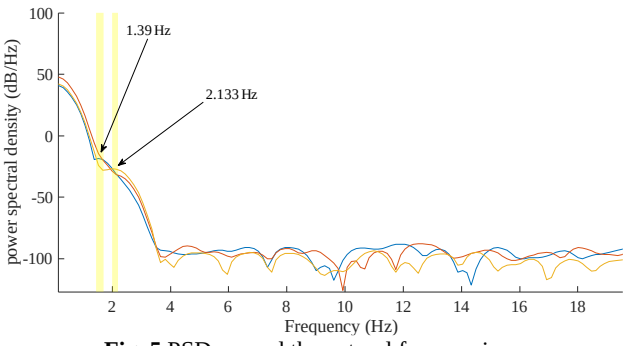

Fig. 5 PSD around the natural frequencies.

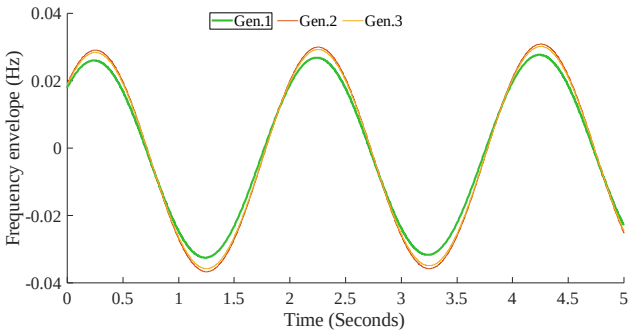

Fig. 7 Generator terminal buses frequency envelopes: Scenario 1.

confidence interval in which the presence of the source frequency (i.e., 0.5 Hz) and its second harmonic (i.e., 1.0 Hz) is seen.

In the following, the energy and multilateral interactive pattern of the generators are shown in Figs. 9 and 10, respectively. Fig. 9 shows that generator one exhibits a completely different behavior. The difference in this behavior is due to the fact that this generator is the source of FOs. Fig. 10 also shows the bilateral behavior of the generators, which is considered as the input of the Laplacian matrix, which subsequently reveals the different behavior of the source one. Fig. 11 shows the source location based on spectral graph theory analysis results. The smallest element corresponding to the eigenvector of the largest eigenvalue, i.e. (-0.80), is related to Generator 1.

4.1.2 Scenario 2: Resonance

The input mechanical torque of generator one was modulated as $\tau_{m_1} = \tau_{m_1}^{o} + 0.1\sin\left(2\pi(1.39)t\right)$. The voltage and frequency envelopes of all generator terminal buses measured by PMUs for this disturbance are shown in Figs. 12 and 13.

As can be seen, none of the amplitudes of the frequency and voltage envelopes oscillation related to the source generator is the maximum. Generator 2 has experienced the most amplitude of both oscillations. The main component (i.e., 1.39 Hz) and the second and third harmonics (i.e., 2.78 and 4.17 Hz) of the voltage amplitude signal are shown in Fig. 14.

In the following, the energy and multilateral interactive pattern of the generators are shown in Figs. 15 and 16, respectively. Fig. 15 shows that generator one exhibits a completely different behavior. The difference in this behavior is due to the fact that this generator is the source of FOs. Fig. 16 also shows the bilateral behavior of the generators, which is considered

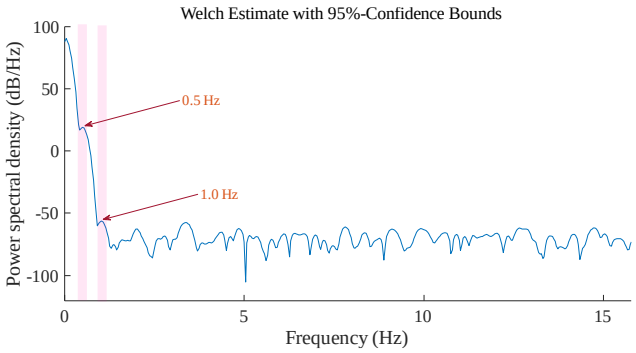

Fig. 8 PSD around the forcing frequency: Scenario 1.

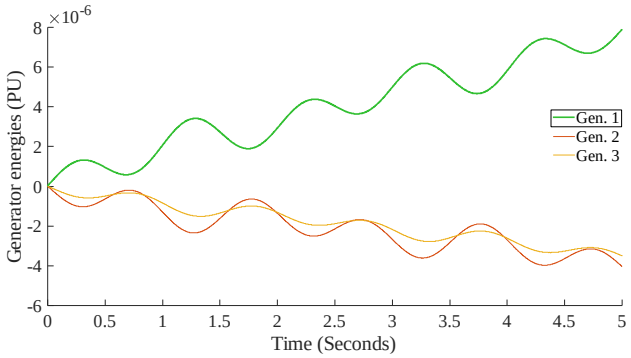

Fig. 9 Generator energy changes: Scenario 1.

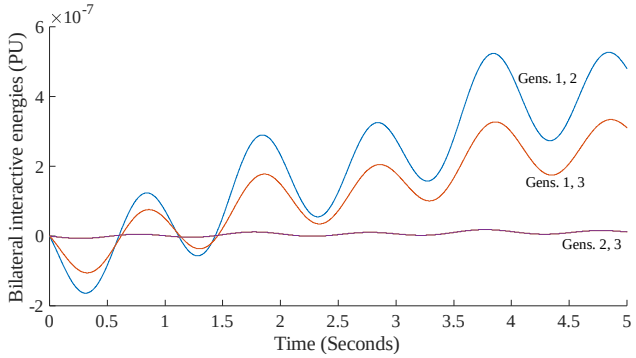

Fig. 10 Multilateral interactive energies: Scenario 1.

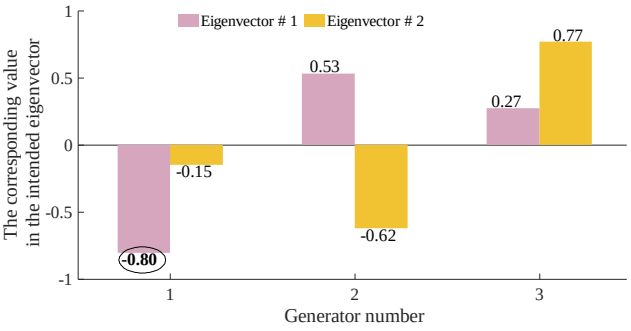

Fig. 11 Target eigenvectors elements: Scenario 1.

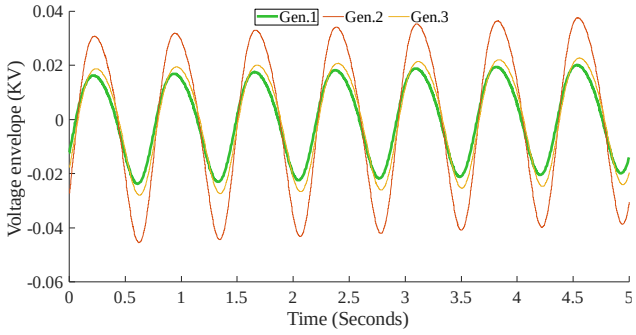

Fig. 12 Generator terminal buses voltage envelopes: Scenario 2.

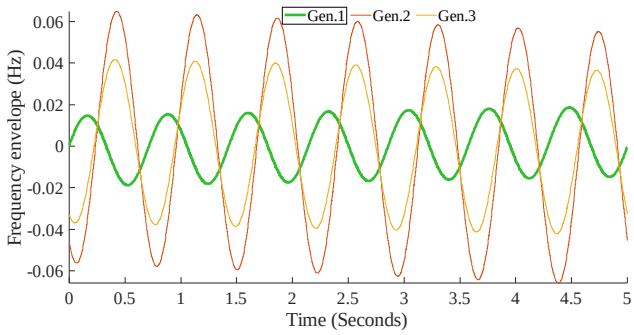

Fig. 13 Generator terminal buses frequency envelopes: Scenario 2.

as the input of the Laplacian matrix, which subsequently reveals the different behavior of the source one. Fig. 17 reveals the source location based on spectral graph theory analysis results. The smallest element corresponding to the eigenvector of the largest eigenvalue, i.e. (-0.73), is related to Generator 1.

4.1.3 Scenario 3: Resonance

The input mechanical torque of generator two was modulated as $\tau_{m_1} = \tau_{m_1}^{o} + 0.1\sin\left(2\pi\left(2.133\right)t\right)$. The voltage and frequency envelopes of all generator terminal buses measured by PMUs for this disturbance are shown in Figs. 18 and 19.

As can be seen, none of the amplitudes of the frequency and voltage envelopes oscillation related to the source generator is the maximum. Generator 3 has experienced the most amplitude of both oscillations. The main component (i.e., 2.133 Hz) and the second and third harmonics (i.e., 4.27 and 6.4 Hz) of the voltage amplitude signal are shown in Fig. 20.

In the following, the energy and multilateral interactive pattern of the generators are shown in Fig. 21 and 22, respectively. Fig. 21 shows that generator two exhibits a completely different behavior. The difference in this behavior is due to the fact that this generator is

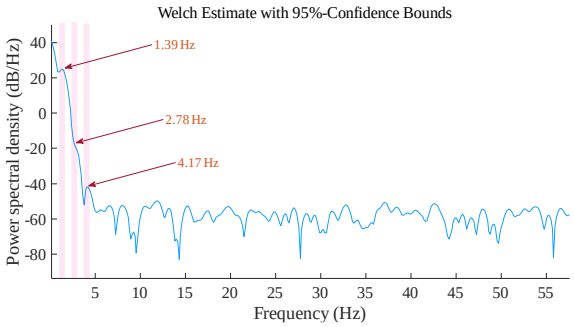

Fig. 14 PSD around the forcing frequency: Scenario 2.

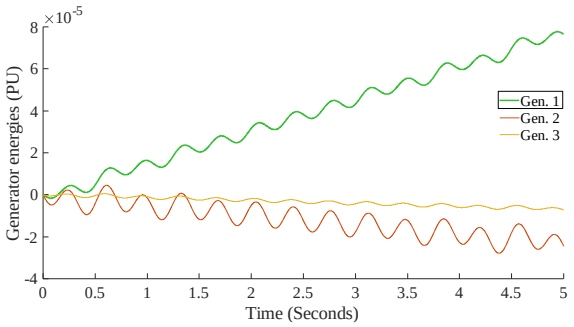

Fig. 15 Generator energy changes: Scenario 2.

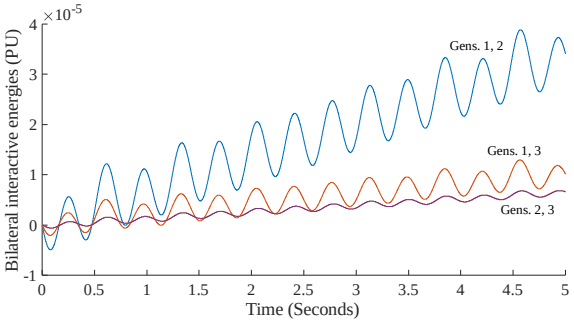

Fig. 16 Multilateral interactive energies: Scenario 2.

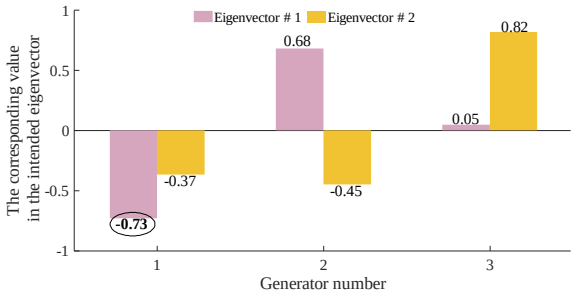

Fig. 17 Target eigenvectors elements: Scenario 2.

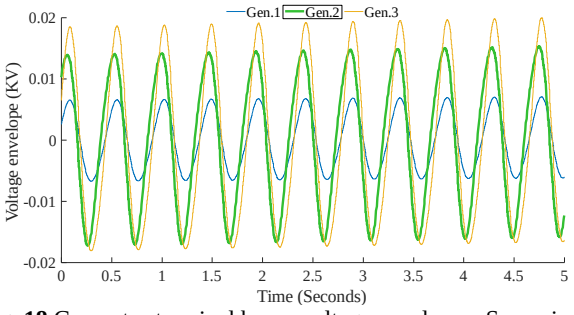

Fig. 18 Generator terminal buses voltage envelopes: Scenario 3.

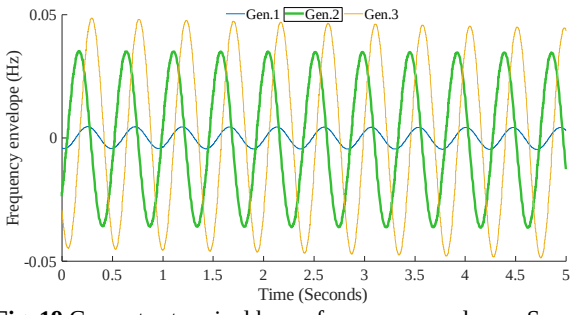

Fig. 19 Generator terminal buses frequency envelopes: Scenario 3.

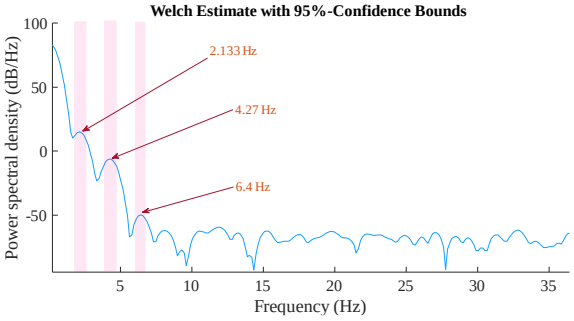

Fig. 20 PSD around the forcing frequency: Scenario 3.

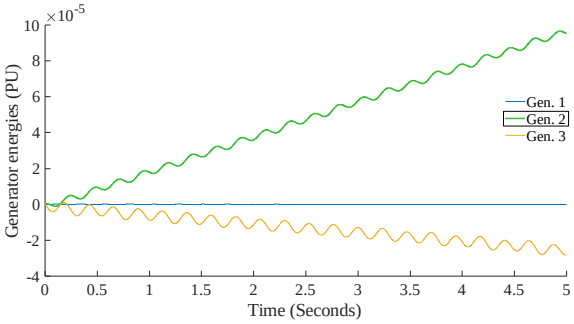

Fig. 21 Generator energy changes: Scenario 3.

the source of FOs. Fig. 22 also shows the bilateral behavior of the generators, which is considered as the input of the Laplacian matrix, which subsequently reveals the different behavior of the source one. Fig. 23 reveals the source location based on spectral graph theory analysis results. The smallest element corresponding to the eigenvector of the second largest eigenvalue, i.e. (-0.69), is related to Generator 2.

4.1.4 Scenario 4: Resonance

The input mechanical torque of Generator 3 was modulated as $\tau_3 = \tau_{m_3}^o + 0.1\sin\left(2\pi(1.39)t\right)$. The voltage and frequency envelopes of all generator terminal buses measured by PMUs for this disturbance are shown in Fig. 24 and 25.

As can be seen, none of the amplitudes of the frequency and voltage envelopes oscillation related to the source generator is the maximum. Generator 2 has experienced the most amplitude of both oscillations. The main component (i.e., 1.39 Hz) and the second and third harmonics (i.e., 2.78 and 4.17 Hz) of the voltage amplitude signal are shown in Fig. 26.

In the following, the energy and multilateral interactive pattern of the generators are shown in Figs. 27 and 28, respectively. Fig. 29 reveals the source location based on spectral graph theory analysis results. The smallest element corresponding to the eigenvector of the second largest eigenvalue, i.e. (-0.72), is related to Generator 3.

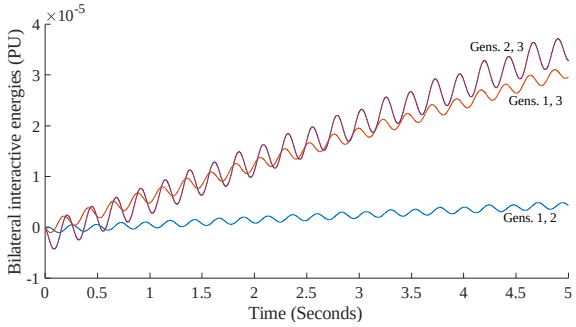

Fig. 22 Multilateral interactive energies: Scenario 3.

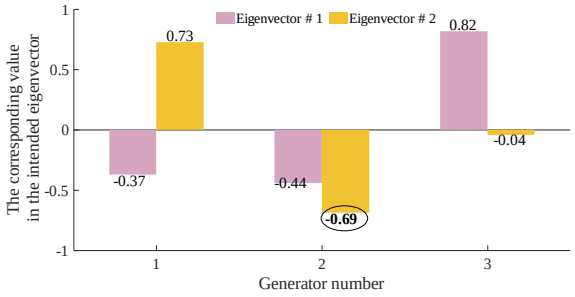

Fig. 23 Target eigenvectors elements: Scenario 3.

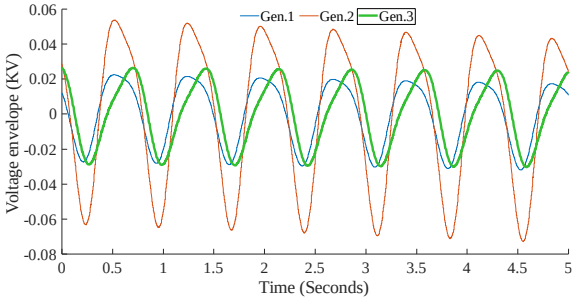

Fig. 24 Generator terminal buses voltage envelopes: Scenario 4.

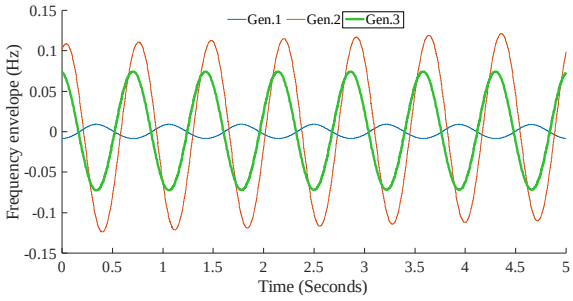

Fig. 25 Generator terminal buses frequency envelopes: Scenario 4.

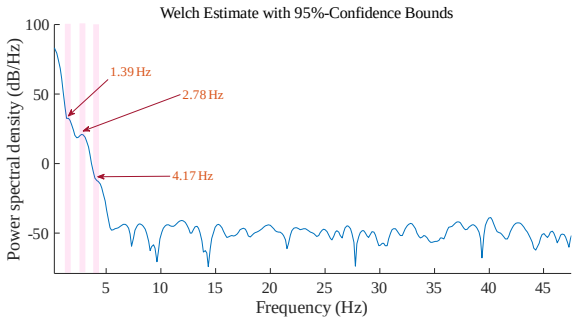

Fig. 26 PSD around the forcing frequency: Scenario 4.

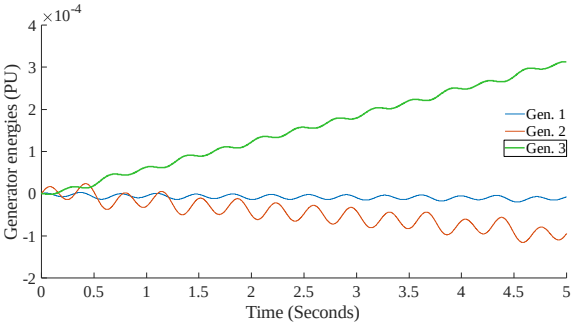

Fig. 27 Generator energy changes: Scenario 4.

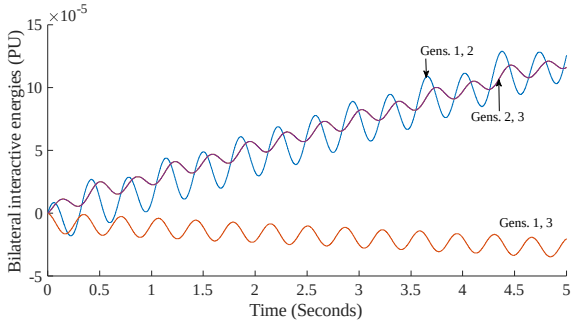

Fig. 28 Multilateral interactive energies: Scenario 4.

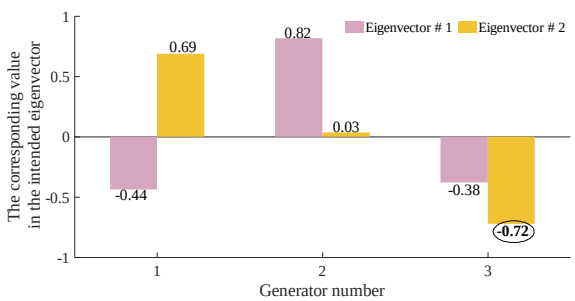

Fig. 29 Target eigenvectors elements: Scenario 4.

4.2 Case Study 2: New England 10-Machine 39-Bus Benchmark Power System

The system one-line diagram and further details can be referred to [9, 18]. It is noted that Generator 1 is the combined equivalent of a large number of physical generators. Following a small signal disturbance in the network, PMU datasets have been used to estimate critical dominant oscillation information. An instantaneous pulse with an amplitude of 0.1 per unit has been injected into the input mechanical torque of Generator 3. Fig. 30 shows the free oscillation of output powers of the generators following this situation.

Spectrum analysis results on the active power signals reveal that the system is dominated by three electromechanical modes: an inter-area mode (with a frequency of 0.6667 Hz) and two local modes (with frequencies of 1.068 Hz and 1.333 Hz), as can be seen in Fig. 31.

4.2.1 Scenario 1: Resonance

The input mechanical torque of generator nine was modulated as $\tau_{m_9} = \tau^{o}_{m_9} + 0.1\sin\left(2\pi(0.6667)t\right)$. The voltage and frequency envelopes of all generator terminal buses measured by PMUs for this disturbance are shown in Figs. 32 and 33.

As can be seen, the amplitude of frequency oscillation related to the source generator is the maximum, but this is not the case for its voltage envelope. Generator 1 has experienced the most amplitude of voltage oscillation. The third harmonic (i.e., 2.0 Hz) of the voltage amplitude signal is shown in Fig. 34.

In the following, the energy pattern of the generators is shown in Fig. 35. Fig. 36 reveals the source location based on spectral graph theory analysis results. The smallest element corresponding to the eigenvector of the largest eigenvalue, i.e. (-0.46), is related to Generator 9.

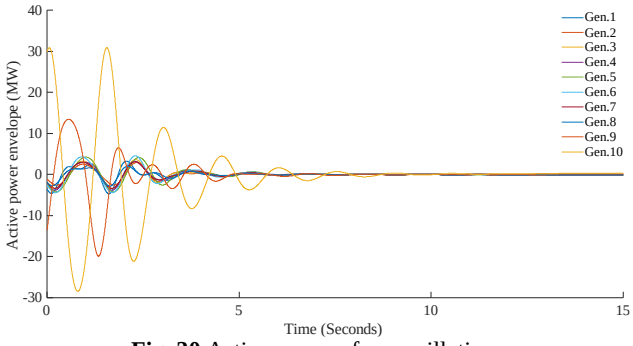

Fig. 30 Active powers free oscillation.

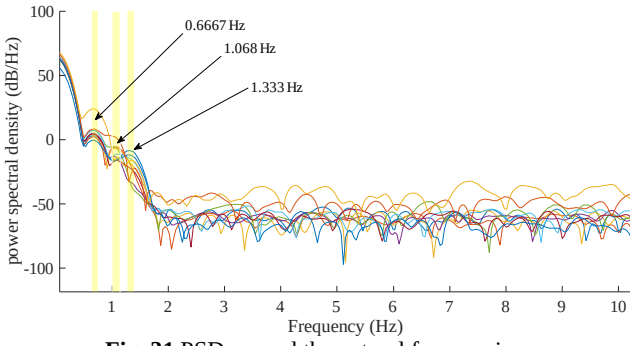

Fig. 31 PSD around the natural frequencies.

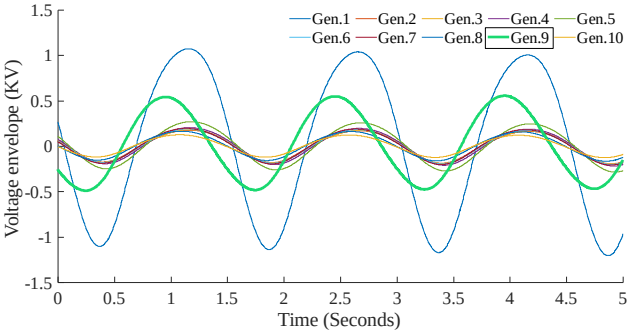

Fig. 32 Generator terminal buses voltage envelopes: Scenario 1.

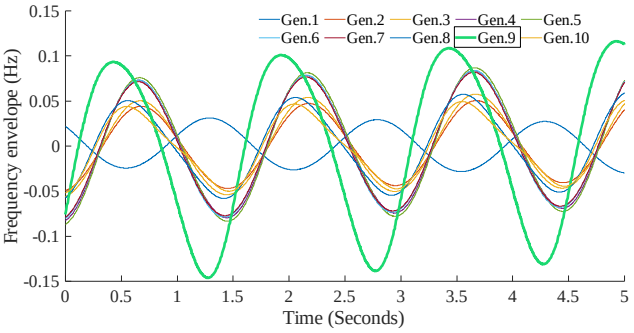

Fig. 33 Generator terminal buses frequency envelopes: Scenario 1.

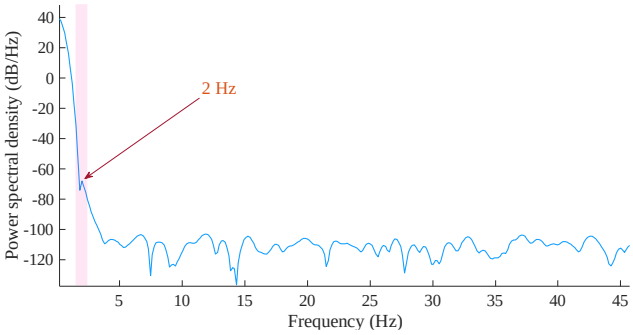

Fig. 34 PSD around the forcing frequency: Scenario 1.

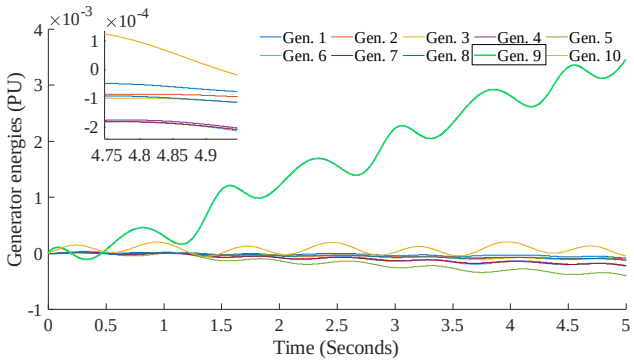

Fig. 35 Generator energy changes: Scenario 1.

4.2.2 Scenario 2: Limit Cycle

Generator 3 Exciter Model is changed to BBSEX1, while the rest are the IEEE type 1 excitation system. We have reduced the generator three exciter's upper bound to a specific value of 2.2847871875 (This number is obtained by trial and error) and set its AVR gain to 10. A three-phase symmetric fault has occurred in the meantime with 0.16s duration. The formation process of the limit cycle can be observed in Fig. 37.

It can be seen that persistent and harmonic oscillations appear about 36 seconds after fault clearance. The voltage and frequency envelopes of all generator terminal buses measured by PMUs are shown in Figs. 38 and 39.

As can be seen, the amplitude of frequency oscillation related to the source generator is the maximum, but this is not the case for its voltage envelope. Generator 6 has experienced the most amplitude of frequency oscillation. The main component (i.e., 1.8 Hz) and the second to eighth harmonics (i.e., 3.6, 5.4, 7.2, 9.0, 10.8, 12.6, and 14.4 Hz) of the voltage amplitude signal are shown in Fig. 40.

In the following, the energy pattern of the generators is shown in Fig. 41. Fig. 42 reveals the source location based on spectral graph theory analysis results. The smallest element corresponding to the eigenvector of the largest eigenvalue, i.e. (-0.94), is related to Generator 3.

4.2.3 Scenario 3: Resonance

The input mechanical torque of generator six was modulated as $\tau_{m_6} = \tau^{o}_{m_6} + 0.1\sin\left(2\pi(1.333)t\right)$. The voltage and frequency envelopes of all generator terminal buses measured by PMUs for this disturbance are shown in Figs. 43 and 44.

As can be seen, the amplitude of frequency oscillation related to the source generator is the maximum, but this is not the case for its voltage envelope. Generator 1 has experienced the most amplitude of voltage oscillation. The main component (i.e., 1.333 Hz) and the second and third harmonics (i.e., 2.67 and 4.0 Hz) of the voltage amplitude signal are shown in Fig. 45.

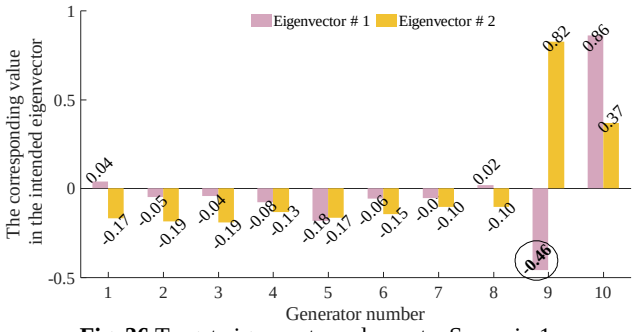

Fig. 36 Target eigenvectors elements: Scenario 1.

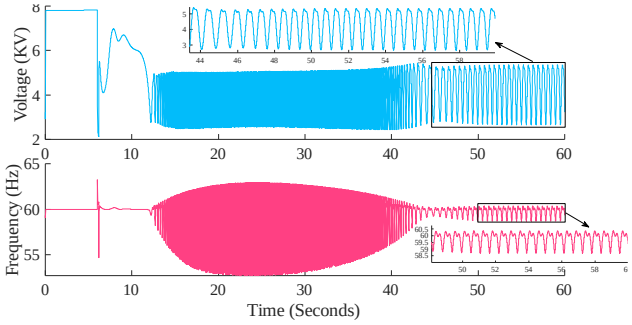

Fig. 37 Limit cycle formation in Scenario 2.

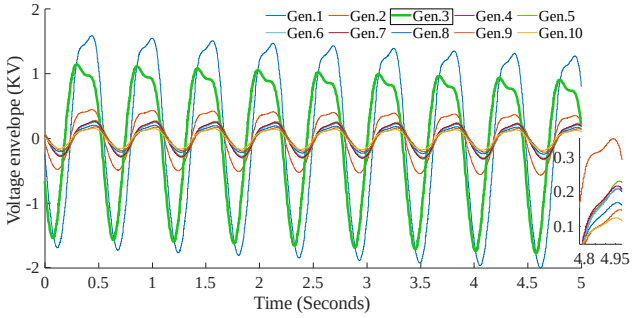

Fig. 38 Generator terminal buses voltage envelopes: Scenario 2.

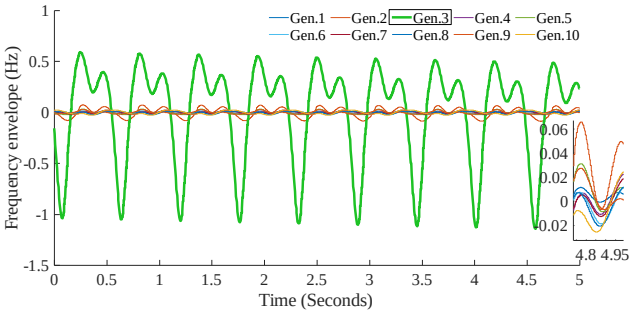

Fig. 39 Generator terminal buses frequency envelopes: Scenario 2.

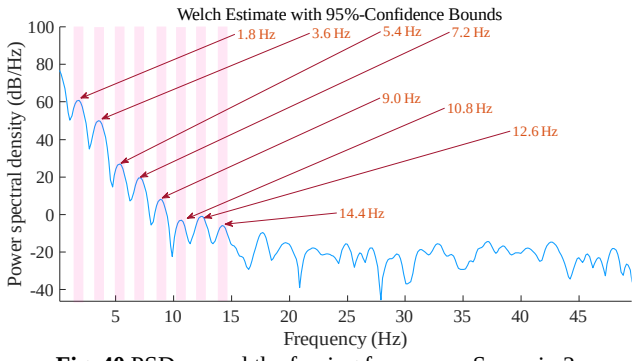

Fig. 40 PSD around the forcing frequency: Scenario 2.

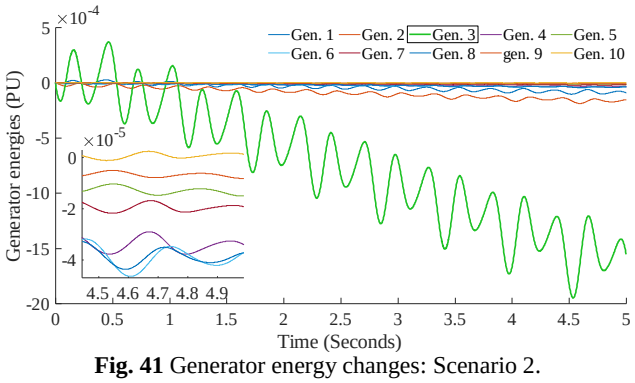

Fig. 41 Generator energy changes: Scenario 2.

In the following, the energy pattern of the generators is shown in Fig. 46. Fig. 47 reveals the source location based on spectral graph theory analysis results. The smallest element corresponding to the eigenvector of the largest eigenvalue, i.e. (-0.94), is related to Generator 6.

4.2.4 Scenario 4: Resonance

The input mechanical torque of generator number 2 was modulated as $\tau_{m_2} = \tau^{o}_{m_2} + 0.1\sin\left(2\pi(1.333)t\right)$. The voltage and frequency envelopes of all generator terminal buses measured by PMUs for this disturbance are shown in Figs. 48 and 49.

As can be seen, none of the amplitude of voltage and frequency oscillations related to the source generator is the maximum. Generator 1 has experienced the most amplitude of voltage oscillation; on the other hand, Generators 6 and 7 experience the most amplitude of frequency oscillations. The main component (i.e., 1.333 Hz) and the second to fifth harmonics (i.e., 2.67, 4.0, 5.33, 6.67, and 8.0 Hz) of the voltage amplitude signal are shown in Fig. 50.

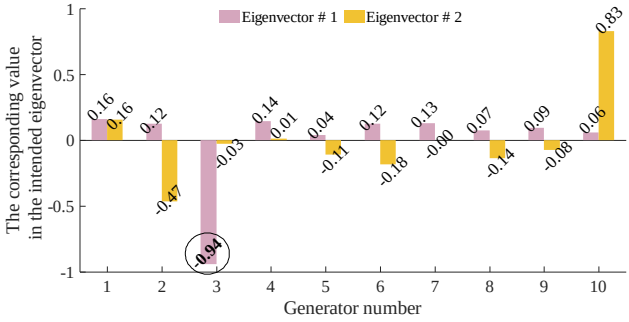

Fig. 42 Target eigenvectors elements: Scenario 2.

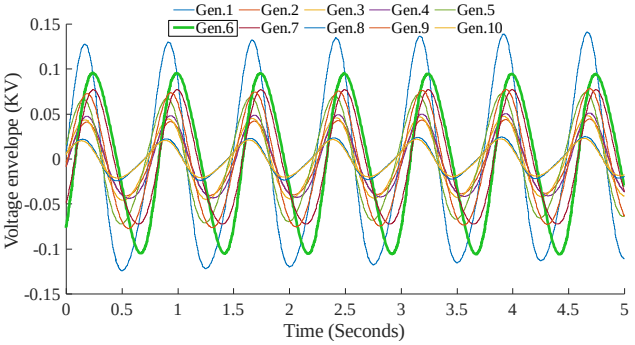

Fig. 43 Generator terminal buses voltage envelopes: Scenario 3.

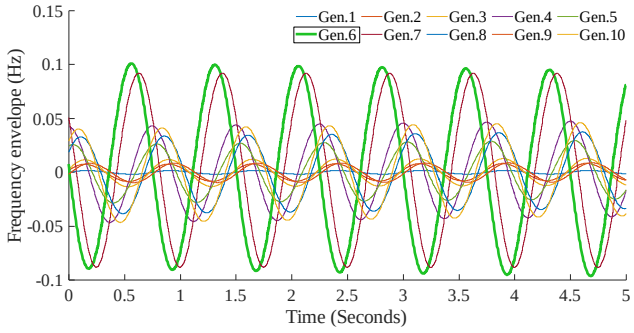

Fig. 44 Generator terminal buses frequency envelopes: Scenario 3.

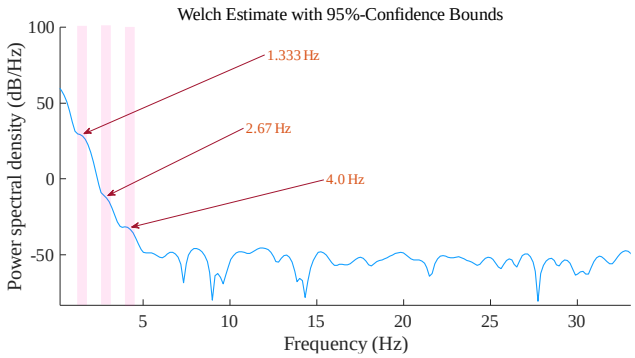

Fig. 45 PSD around the forcing frequency: Scenario 3.

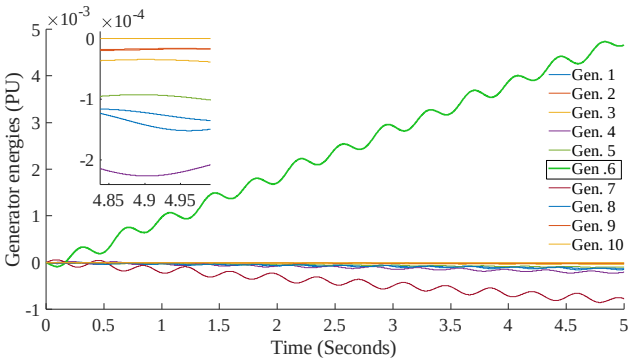

Fig. 46 Generator energy changes: Scenario 3.

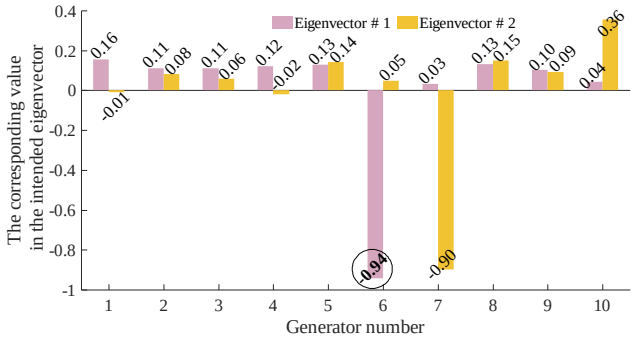

Fig. 47 Target eigenvectors elements: Scenario 3.

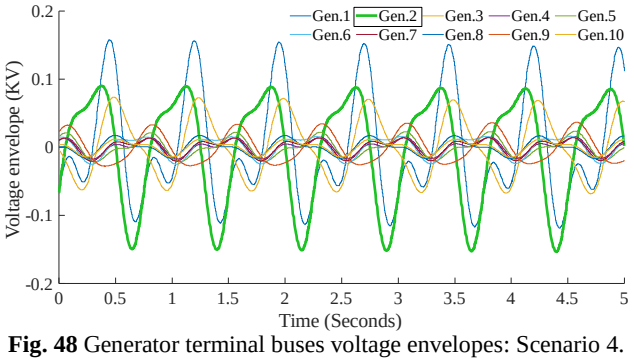

Fig. 48 Generator terminal buses voltage envelopes: Scenario 4.

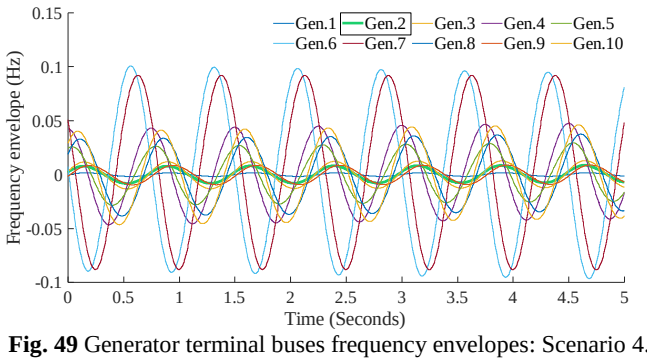

Fig. 49 Generator terminal buses frequency envelopes: Scenario 4.

In the following, the energy pattern of the generators is shown in Fig. 51. Fig. 52 reveals the source location based on spectral graph theory analysis results. The minor element corresponding to the eigenvector of the largest eigenvalue, i.e., -0.94, is related to Generator 2.

4.2.5 Scenario 5: Resonance

The input mechanical torque of generator five was modulated as $\tau_{m_5} = \tau^{o}_{m_5} + 0.05\sin\left(2\pi(1.068)t\right)$. The voltage and frequency envelopes of all generator terminal buses measured by PMUs for this disturbance are shown in Fig. 53 and 54.

As can be seen, the amplitude of voltage and frequency oscillations related to the source generator is larger than the rest. The main component (i.e., 1.068 Hz) and the second to fifth harmonics (i.e., 2.136, 3.2, 4.273, and5.34 Hz) of the voltage amplitude signal are shown in Fig. 55.

In the following, the energy pattern of the generators is shown in Fig. 56. Fig. 57 reveals the source location based on spectral graph theory analysis results. The smallest element corresponding to the eigenvector of the largest eigenvalue, i.e., -0.94, is related to Generator 5.

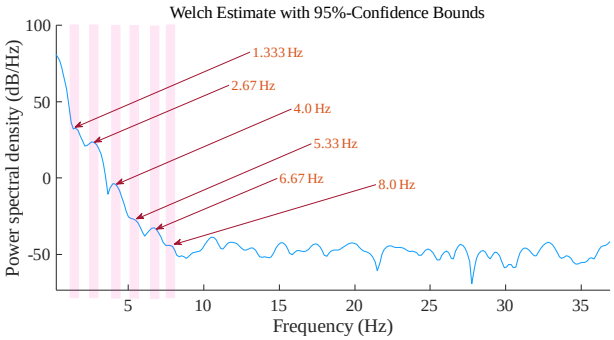

Fig. 50 PSD around the forcing frequency: Scenario 4.

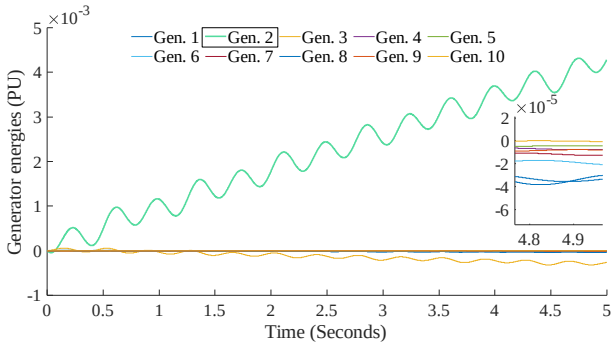

Fig. 51 Generator energy changes: Scenario 4.

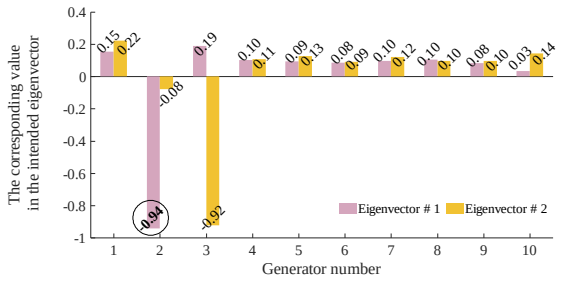

Fig. 52 Target eigenvectors elements: Scenario 4.

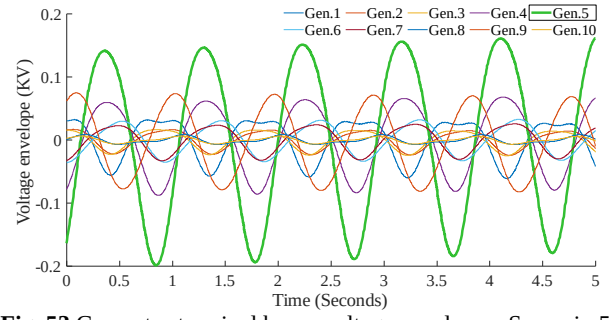

Fig. 53 Generator terminal buses voltage envelopes: Scenario 5.

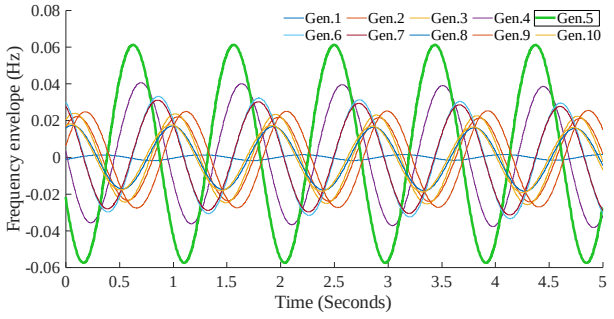

Fig. 54 Generator terminal buses frequency envelopes: Scenario 5.

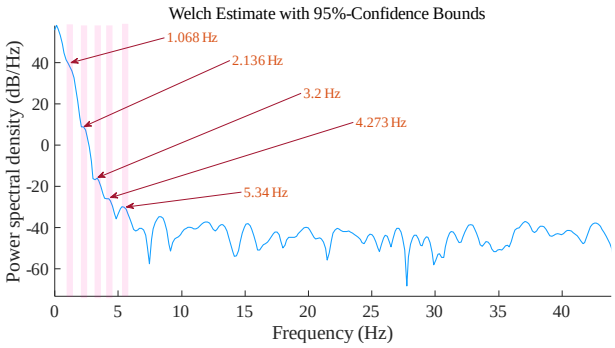

Fig. 55 PSD around the forcing frequency: Scenario 5.

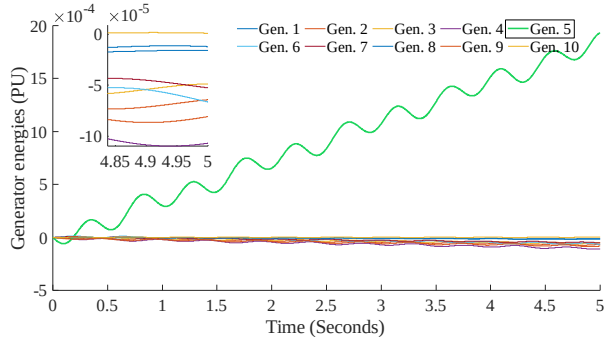

Fig. 56 Generator energy changes: Scenario 5.

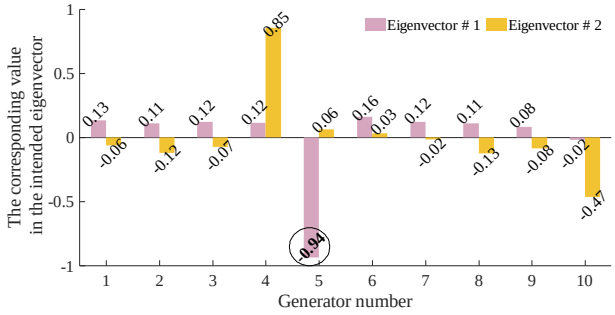

Fig. 57 Target eigenvectors elements: Scenario 5.

As shown, the proposed approach can accurately pinpoint the location of the FOs source even around the oscillatory mode frequencies and limit cycle conditions.

5 Conclusion

In this paper, we have proposed a new energy-driven approach to address the source of FOs in nearly real-time. As soon as the presence of FOs in the power system is detected, an appropriate set of quantitative measures have been extracted through a well-established multilateral interactive pattern among synchronous generators. In the next step, these indicators have been utilized to construct a complete positive weighted undirected graph. After that, a normalized Laplacian matrix has been achieved based on spectral graph theory. The associated eigenvalue spectrum was investigated to expose any anomalous patterns with high efficiency.

Furthermore, the presented approach illustrates a satisfactory and reliable performance in locating the source of FOs under problematic resonance conditions. In the entire procedure, no simplification assumptions are made regarding network losses. All desirable real-time measurements have been obtained using PMUs with a reporting rate of 60 samples per second installed at all generators' terminals. The proposed methodology has been evaluated on the WECC 3-machine 9-bus and New England 10-machine 39-bus benchmark power systems modeled in the RTDS Simulator. The results obtained through the simulations performed in the MATLAB environment demonstrate the capability of the presented framework to address the FOs source location problem considering real-world constraints.

The energy method mainly focuses on the oscillating sources of the generator side. Such a multilateral approach should also be developed for cyclic loads. It is suggested that in future research, FOs originated and the result of the interaction of several sources (a combination of generation and load sides) be considered by researchers.

Intellectual Property

The authors confirm that they have given due consideration to the protection of intellectual property associated with this work and that there are no impediments to publication, including the timing of publication, with respect to intellectual property.

Funding

No funding was received for this work.

CRediT Authorship Contribution Statement

A. Hesami Naghshbandy: Idea & conceptualization, Research & investigation, Data curation, Methodology, Project administration, Supervision, Verification, Original draft preparation, Revise & editing. **K. Naderi:** Idea & conceptualization, Research & investigation, Data curation, Analysis, Methodology, Software and simulation, Verification, Original draft preparation. **U. Annakkage:** Research & investigation, Methodology, Project administration, Software and simulation, Supervision, Verification, Original draft preparation, Revise & editing.

Declaration of Competing Interest

The authors hereby confirm that the submitted manuscript is an original work and has not been published so far, is not under consideration for publication by any other journal and will not be submitted to any other journal until the decision will be made by this journal. All authors have approved the manuscript and agree with its submission to "Iranian Journal of Electrical and Electronic Engineering".

References

[1] A. Monti, C. Muscas, and F. Ponci, *Phasor measurement units and wide area monitoring systems*. Academic Press, 2016.

[2] M. Ghorbaniparvar, "Survey on forced oscillations in power system," *Journal of Modern Power Systems and Clean Energy*, Vol. 5, No. 5, pp. 671–682, 2017.

[3] P. B. Reddy and I. A. Hiskens, *Limit-induced stable limit cycles in power systems*. IEEE, 2005.

[4] G. Anagnostou and B. C. Pal, "Impact of overexcitation limiters on the power system stability margin under stressed conditions," *IEEE Transactions on Power Systems*, Vol. 31, No. 3, pp. 2327–2337, 2015.

[5] D. Wu, P. Vorobev, S. C. Chevalier, and K. Turitsyn, "Modulated oscillations of synchronous machine nonlinear dynamics with saturation," *IEEE Transactions on Power Systems*, Vol. 35, No. 4, pp. 2915–2925, 2019.

[6] M. Liu, F. Bizzarri, A. M. Brambilla, and F. Milano, "On the impact of the dead-band of power system stabilizers and frequency regulation on power system stability," *IEEE Transactions on Power Systems*, Vol. 34, No. 5, pp. 3977–3979, 2019.

[7] D. Lathrop, "Nonlinear dynamics and chaos: With applications to physics, biology, chemistry, and engineering," *Physics Today*, Vol. 68, No. 4, p. 54, 2015.

[8] S. A. N. Sarmadi, V. Venkatasubramanian, and A. Salazar, "Analysis of November 29, 2005 western American oscillation event," *IEEE Transactions on Power Systems*, Vol. 31, No. 6, pp. 5210–5211, 2016.

[9] M. Pai, *Energy function analysis for power system stability*. Springer Science & Business Media, 2012.

[10] L. Chen, Y. Min, and W. Hu, "An energy-based method for location of power system oscillation source," *IEEE Transactions on Power Systems*, Vol. 28, No. 2, pp. 828–836, 2012.

[11] Y. Shu, X. Zhou, and W. Li, "Analysis of low frequency oscillation and source location in power systems," *CSEE Journal of Power and Energy Systems*, Vol. 4, No. 1, pp. 58–66, 2018.

[12] S. Maslennikov, B. Wang, and E. Litvinov, "Dissipating energy flow method for locating the source of sustained oscillations," *International Journal of Electrical Power & Energy Systems*, Vol. 88, pp. 55–62, 2017.

[13] R. Jha and N. Senroy, "Forced oscillation source location in power systems using system dissipating energy," *IET Smart Grid*, Vol. 2, No. 4, pp. 514–521, 2019.

[14] K. Kirihara, J. Yamazaki, P. Chongfuangprinya, S. Konstantinopoulos, C. Lackner, J. H. Chow, S. Maslennikov, and Y. Liu, "Speeding up the dissipating energy flow based oscillation source detection," in *IEEE International Conference on Smart Grid Synchronized Measurements and Analytics (SGSMA)*, pp. 1–8, 2019.

[15] P. W. Sauer, M. A. Pai, and J. H. *Chow, Power system dynamics and stability: with synchrophasor measurement and power system toolbox*. John Wiley & Sons, 2017.

[16] B. Nica, "A brief introduction to spectral graph theory," *arXiv preprint arXiv:1609.08072*, 2016.

[17] V. Vittal, J. D. McCalley, P. M. Anderson, and A. Fouad, *Power system control and stability*. John Wiley & Sons, 2019.

[18] T. Athay, R. Podmore, and S. Virmani, "A practical method for the direct analysis of transient stability," *IEEE Transactions on Power Apparatus and Systems*, No. 2, pp. 573–584, 1979.

A. Hesami Naghshbandy received a B.Sc. (1994), M.Sc. (2000), and Ph.D. (2008) in Electrical Engineering from Iran University of Science and Technology (IUST), Tehran, Iran. His research interests include power systems dynamics, stability and security and power systems operation and control. Currently, he is an Associate Professor at the Electrical Engineering Department of the University of Kurdistan, Sanandaj, Iran, and an active member of both the IEEE and CIGRE.

K. Naderi received B.Sc. (2012) and M.Sc. (2015) degrees in Electrical Engineering from Razi University, and the University of Kurdistan. He is currently pursuing a Ph.D. in Electrical Engineering from the University of Kurdistan. He is a Visiting Doctoral Researcher at the Power Systems Dynamics and Control Laboratory of the University of Manitoba, Winnipeg, MB, Canada. His research interests include power systems dynamics, stability, security assessment and wide-area monitoring, protection and control (WAMPAC), and signal processing algorithms and techniques to solve challenging problems in power systems.

U. D. Annakkage (SM'04) received a B.Sc. (Eng.) degree in Electrical Engineering from the University of Moratuwa, Moratuwa, Sri Lanka, in 1982, and the M.Sc. and Ph.D. degrees in Electrical Engineering from the University of Manchester Institute of Science and Technology (UMIST), Manchester, U.K., in 1984 and 1987, respectively. Currently, he is a Professor at the University of Manitoba, Winnipeg, MB, Canada. He was the Head of the Electrical and Computer Engineering Department, University of Manitoba, from 2008 to 2012. He was an editor for the IEEE Transactions on Power Systems from 2009 to 2012. Currently, he is the Convener of the CIGRE Working Group on the Application of Phasor Measurement Units for monitoring power system dynamic performance. His research interests include power system stability and control, security assessment and control, operation of restructured power systems, and power system simulation.